

Local detection of X-ray spectroscopies with an in-situ Atomic Force Microscope

M.S. Rodrigues,^{a*} O. Dhez,^a S. Le Denmat,^a J. Chevrier,^b R. Felici^a and F. Comin^a

^aEuropean Synchrotron Radiation Facility,
Grenoble, France

^bInstitut Néel CNRS/UJF,
Grenoble, France

E-mail: mario.rodrigues@esrf.fr

ABSTRACT: The in situ combination of Scanning Probe Microscopies with X-ray microbeams adds a variety of new possibilities to the panoply of synchrotron radiation techniques. This paper describes an optics-free Atomic Force Microscope that can be directly installed on most of the synchrotron radiation end-stations for combined X-ray and atomic force microscopy experiments. The instrument can be used for atomic force imaging of the investigated sample or to locally measure the X-ray absorption or diffraction, or it can also be used to mechanically interact with the sample while simultaneously taking spectroscopy or diffraction measurements. The local character of these measurements is intrinsically linked with the use of the Atomic Force Microscope tip. It is the sharp tip that gives the opportunity to measure the photons flux impinging on it, or to locally measure the absorption coefficient or the shape of the diffraction pattern. At the end an estimation of the limits of the various techniques presented is also discussed.

KEYWORDS: Interaction of radiation with matter; Photoemission; Beam-line instrumentation (beam position and profile monitors; beam-intensity monitors; bunch length monitors); X-ray diffraction detectors.

*Corresponding author.

Contents

1. Introduction	1
2. Experimental set up	2
3. Microbeam interaction with a metallic tip	4
4. Tip detection of X-rays absorption	6
5. Tip measurement of the diffraction	8
6. Perspectives	10

1. Introduction

Scanning Probe Microscopy (SPM) techniques are used in many scientific fields ranging from biology to materials sciences. Nowadays, they are thought to be at the heart of nanoscience. SPMs are easy to use, produce high resolution images of the sample and unveil many *local* properties of the surface. Synchrotron Radiation, on its side, is used to probe the atomic and electronic structures but *averaging* over the illuminated volume. In the most recent years the use of micro and nano X-ray beams is steadily increasing and the joint exploitation of SPM and Synchrotron Radiation techniques seems ever more desirable.

In micro-nano characterization it is often necessary to work on a single object whose size can vary from the micro to the nanoscale. For more systematic and comprehensive exploration of the micro-nano world, it is covetable to perform SPM and X-ray experiments on the same single object in the same conditions and at the same time.

To accomplish this, some paths have already been explored. A first one consisted in combining Scanning Tunneling Microscopy [1] with X-ray beams in an intent to provide chemical contrast in near field microscopies [2]. This was done by installing an Ultra High Vacuum Scanning Tunneling Microscope on a dedicated X-ray beam line [3–5]. According to the authors, X-rays induce changes in the tunneling probability adding then chemical contrast of the order of tens of nanometers to the usual topographic resolution of a Scanning Tunneling Microscope.

A different approach was taken by Ishii [6], who has combined X-ray absorption with Scanning Capacitance Microscopy [7] to probe localized charges. This last technique parallels Electrostatic Force Microscopy [8] and Kelvin Probe Microscopy [9], both belonging to the family of the Atomic Force Microscopies [10].

Due to the versatility of the Atomic Force Microscope (AFM) [11], we considered an extensive integration of SPM techniques on synchrotron radiation beam lines in order to combine them

indifferently with diffraction or with spectroscopy experiments. For this purpose, we adapted compact, optics free AFM instruments to typical end stations. We have also used the tip as a nanomanipulation tool for sample interaction under X-ray beams. The AFM can also be operated in its Magnetic Force Microscopy mode [12] to image individual magnetic domains and perform local spectroscopy even if X-ray beams are bigger than domain dimensions. The experiments described here have been conducted at the European Synchrotron Radiation Facility, in the framework of the X-Tip European Project [13].

The work aimed to explore versatility, ease of use and the extent of the applications spectrum. The difficulties to overcome involved essentially issues of stability and alignment, since on the one hand the beamline environment is not devoid of mechanic vibrations and on the other hand, the alignment of tip, sample and microbeam should be a routine procedure for an easy exploitation of the instrument. As a general reference, beamlines that do not need a diffractometer are stable enough to allow a vertical resolution of 1 nm or 2 nm. On diffractometer based beamlines, this value can increase to about 20 nm, depending on the particular setup.

To solve the problem of alignment, the AFM tip has been used as a beam position monitor. Conversely, the tip can be used as a local absorption and diffraction detector. The lateral resolution in this case is still rather limited, due to the technical difficulty of producing coaxial tips bare just on their apex. Although not described in this paper, a reliable method for preparing tips that leave a submicrometer open metallic apex is now being developed. We call these "Smart Tips". Once this task is accomplished, a lateral resolution better than 50 nm is expected. The main underlying idea is that tip-mediated detection is intrinsically localized to the area "seen" by the tip (few nm) even if the beam is spread over a much wider sample area.

The microscope we developed operates very much like a conventional AFM but with a simplified (and more robust) set up. In conventional AFMs, the deflection of the cantilever is detected by measuring with a Position Sensitive Photodetector the position of a laser beam reflected by the back of the cantilever. The deflection of this beam is function of the bending of the cantilever. In contrast, the AFM presented here is based on a quartz tuning fork (TF). Because quartz exhibits natural piezoelectricity, this solution allows direct detection of the motion of the oscillator since its alternating stress field is converted into alternating charge i.e., current. The use of TFs in SPM design has been the subject of a vast and fast growing literature [14 – 16].

2. Experimental set up

Figure 1 shows the experimental set up. The TF with a tungsten tip glued on one of its extremities is mechanically mounted on an aluminum support provided with a piezoelectric block for the mechanical excitation of the TF. A phase locked loop (PLL) supplies the excitation signal and detects the resonance frequency and amplitude of the oscillating fork. The change in resonance frequency is the input of a feedback loop used to obtain the topography of the surface.

A slotted rotating wheel (chopper) modulates the intensity of the beam at a frequency between 1 kHz and 5 kHz. A lock-in is used to synchronously detect the current induced on the tip. This current is the result of either sample or tip photoemitted electrons.

The tungsten tip is mounted on the TF by means of a conductive glue to ensure the electrical connection with one of the TF electrodes. The preparation process consists of two steps. First, a

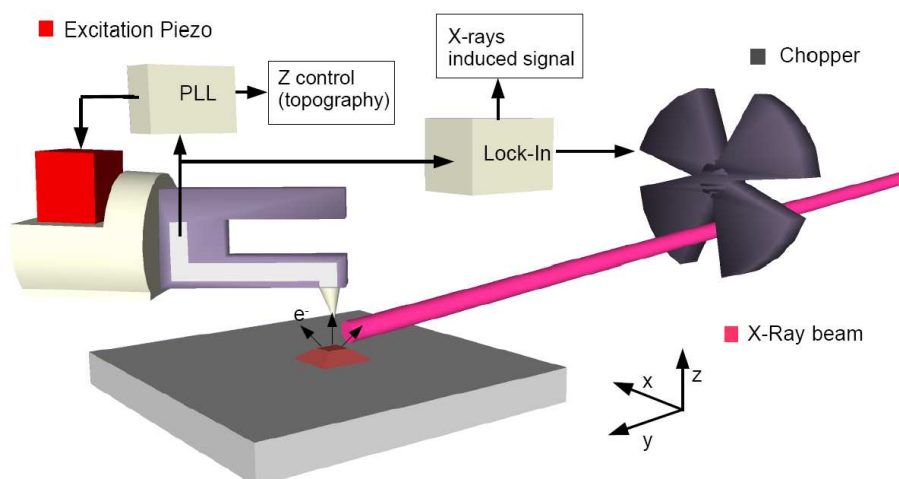


Figure 1. Experimental setup: a TF is used as the tip-sample force gradient transducer; a feedback loop is used to control the tip-sample distance by keeping the resonance frequency of the TF constant, while the tip scans over the sample resulting in a topographical image. A conductive tip is used to detect the time modulated X-ray induced signal i.e., tip or sample photoelectrons.

tungsten wire with $100\ \mu\text{m}$ diameter and 2 cm long is glued on the TF and in a second step the tip is chemically etched with potassium hydroxide as explained in [17]. Typical natural frequency of a TF after tip mounting is around 30 kHz.

The total current collected by the TF electrode is the sum of the TF piezoelectric signal and the X-ray induced currents. Their respective contributions are separated by the phase locked loop and the lock-in amplifier respectively, after appropriate amplification by a transimpedance preamp with a gain of $10^7\ \Omega$.

The use of a quartz TF offers several advantages. Among them the fact that quartz naturally exhibits piezoelectricity making it straightforward to detect its motion. An oscillation of 1 nm results in a current of about 2 nA or 20 mV after the preamp. A second advantage reates to the fact that neither a laser nor a photodetector are necessary for the operation of this type of AFM microscopes simplifying their installation on beamlines and making them more robust. The third advantage comes from the fact that TFs are much bigger than usual cantilevers making them easier to handle and to image, which is quite handy when aligning the X-ray with the tip.

TFs have then a very high quality factor ($Q \approx 8000$ versus $Q \approx 30$ for a conventional cantilever) or in other words, a very small bandwidth. The Q factor is defined as $f/\Delta f$ with f the TF resonance frequency and Δf the Full Width at Half Maximum of the Lorentzian resonance curve. It measures how many cycles the system must undergo until it relaxes to equilibrium. Its small bandwidth acts then as a filter to external noise since only excitation frequencies within a very small frequency window of ≈ 5 Hz can induce perturbations. For comparison, in a conventional AFM cantilever at room conditions the window is of 700 Hz.

Due to the size of a TF prong, the spring constant or stiffness, k , is much higher than that of a conventional AFM cantilever, typically $\approx 20.000\ \text{N/m}$ versus $40\ \text{N/m}$. However, in dynamic mode, the sensitivity depends on the dynamic stiffness defined as k/Q . The frequency shift due to the inter-

action is directly proportional to the stiffness of the cantilever. However, the center frequency of an oscillator with high Q factor is better defined and consequently smaller frequency shifts can be measured. The dynamic stiffness for a conventional AFM silicon cantilever or a TF is roughly the same.

The high Q factor of the TF, or alternatively the long relaxation time has led us to choose phase locked loop detection of the TF oscillations. This is because the relaxation time of the TF plus phase locked loop is smaller than that of the TF alone. The phase locked loop measures the phase difference between the excitation force in input to the TF and the oscillation in return. At resonance, the oscillation follows the excitation with a phase difference of -90° . The phase loop increases or decreases the excitation frequency in order to maintain this phase difference constant. In this way it assures that the TF is always at its resonance frequency even when interacting with the sample. For instance, at few nm from the sample (≈ 5 nm) the resonance frequency of the fork shifts to lower values because of the attractive van der Waals forces. The phase loop detects this frequency shift by measuring the phase shift between the oscillation and the excitation and adjusts the excitation frequency to get back the preset -90° . Thus, while interacting, the excitation frequency is equal to the *interacting* resonance frequency which is slightly lower than the *free* resonance frequency.

The difference between the *free* resonance frequency and the *interacting* resonance frequency is used in turn as the input of a second loop used to obtain the topography. This second loop changes the sample position in such a way that the *interacting* resonance frequency is kept constant.

The X-ray beam used to obtain the results presented below had 10^{12} photons per second in about 10^{-4} bandpass on about $4 \times 4 \mu\text{m}^2$ at normal incidence.

3. Microbeam interaction with a metallic tip

The first step of the experiment consists in aligning the beam with the tip of the AFM. The Total Electron Yield (TEY) i.e., the current given by the integrity of the photoemitted electrons regardless of their kinetic energy is systematically recorded as the tip is moved in the XZ plane perpendicular to the beam. This produces experimental images of the tip as shown in figure 2a with their respective cross sections in figure 2c.

A characteristic feature of this type of scan is an increase of the TEY when the X-ray beam is at grazing incidence on the tip (see figure 2a and 2b). This higher contrast is due to the limited escape depth of the electrons. At grazing incidence the beam footprint is larger and the X-ray penetration into the bulk lower. Consequently, there will be more electrons produced close to the surface and likely to escape.

The relevant parameters to analyze the experimental results of figure 2a are the absorption length μ_l (which is of few microns for the energy used) and the characteristic energy loss per unit of length i.e., the stopping power $S(E)$ for electrons.

In order to quantify the results, we defined an effective escape depth d_{eff} as the distance after which the electrons have lost kinetic energy to a value below the necessary energy to overcome the vacuum barrier. If a photon is absorbed at a distance d from the surface, smaller than d_{eff} , it may or not give rise to photoemission, depending on the particular trajectories of the electron cascade. Assuming all trajectories are equally possible, there is a spherical surface with radius d_{eff} and center at d , such that in average the photoemitted electrons reach this surface. Then, from

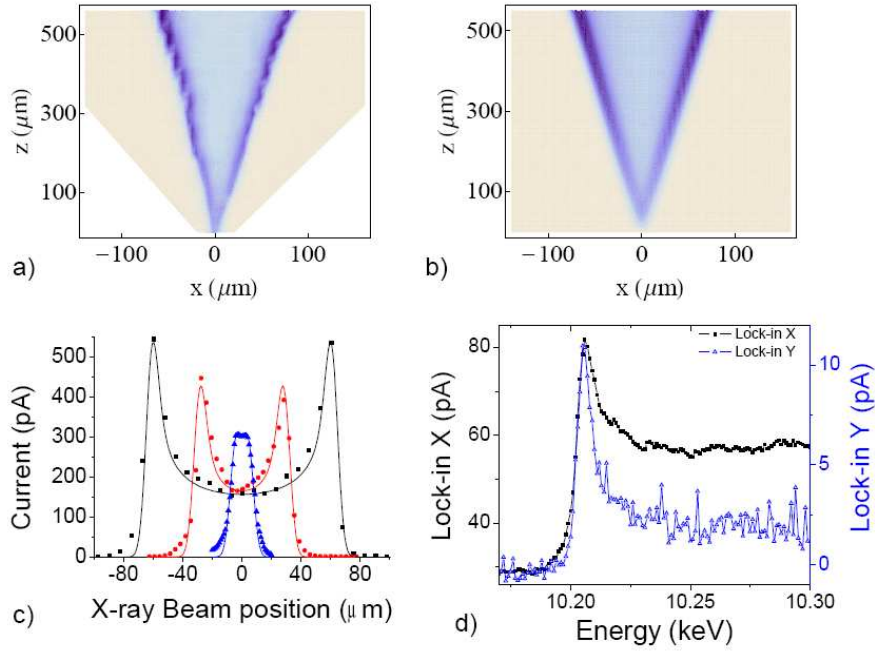


Figure 2. (a) 3D plot of the current flowing to the tip as a function of the position of the beam relative to the tip. (b) Simulation of (a). (c) Cross sections of (a) and (b). (d) Current from the tip as a function of photon energy across the L_3 edge of tungsten.

simple geometrical considerations there is a probability of $1/6$ that a photon absorbed at a distance $d < d_{\text{eff}}$ results in one photoelectron out.

Considering the complexity of the photon absorption processes, their conversion into electrons, and how these electrons lose their kinetic energy, it is clear that such a definition is oversimplified. However, it is sufficient to take into account the experimental results and provide a reasonable analysis.

The intensity of the current $i(x, z)$, was calculated considering a 2D Gaussian beam shape and a linear absorption length on tungsten for 10 keV photons of $\mu = 5.8 \mu\text{m}$. The measured current equals $1/6$ of the number of photons absorbed within a distance smaller than d_{eff} from the surface:

$$i(x, z) = \int \frac{1}{6} I(x, z) f(x, z) \left(1 - e^{-t(x, z)/\mu_l} \right) dx dz. \quad (3.1)$$

$I(x, z)$ is the Gaussian distribution of the photons, $f(x, z)$ takes into account only the number of photons that are absorbed at a distance smaller than d_{eff} from the surface and $t(x, z)$ is the length along which the absorbed photons contribute to produce current. Both $f(x, z)$ and $t(x, z)$ depend on the geometry of the tip as well as on the geometry of the incidence and therefore both depend on the parameter d_{eff} . If the radius of the tip is smaller than d_{eff} then $f = 1$ and $t(x, z)$ is simply the thickness $t = \sqrt{R(z)^2 - x^2}$ with $R(z)$ the radius of the tip at position z . If the radius of the tip is much larger than d_{eff} and the beam is incident on the tip perpendicular to it, then $t(x, z) = d_{\text{eff}}$.

On the basis of this calculation it can now be estimated d_{eff} . Figures 2a, 2b and 2c show the agreement between measured and calculated current versus the tip position relative to the beam. The only adjustable parameter is d_{eff} . All other quantities are derived from experimental conditions.

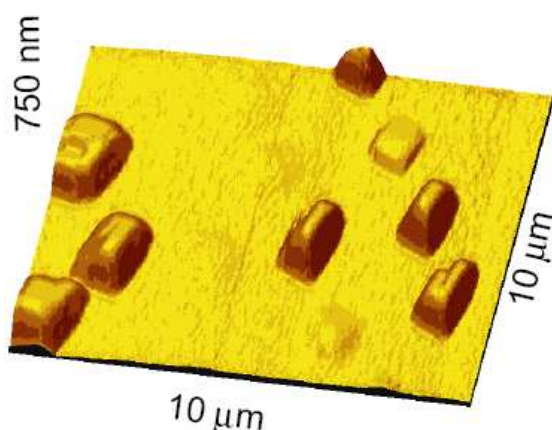


Figure 3. In-situ AFM topography image.

From our experiments, we systematically obtain d_{eff} of about 30 nm or less. This is an important figure since it indicates how deep the surface is probed. Additionally, neglecting any issue of convolution with the tip shape, i.e. assuming a point-like-tip, the best possible resolution in TEY collection cannot be better than this value, that in turn is slightly material dependent.

As a final remark, it seems interesting to point out that additional information is coming from the use of a lock-in to detect the photoemission processes. The lock-in measures only the component of the signal which has the selected specific frequency f (within a bandwidth of about 1Hz). This signal may have a phase lag. The total signal is given by $R \sin(2\pi ft + \phi) = X \sin(2\pi ft) + Y \cos(2\pi ft)$, the *rms* is then given by $R = \sqrt{X^2 + Y^2}$. X is the in-phase contribution while Y is out of phase by $\pi/2$. The absorption and emission processes happen in a time scale ($< ns$) much smaller than $1/f$ ($\approx 100 \mu s$), thus the signal is expected to be in phase or to lag by π depending on whether electrons are emitted *from* the tip or *into* the tip. In figure 2d the L_3 edge of tungsten is seen both in the X and Y lock-in signals. Y has a value close to zero along all the scan except at the white line peak. Thus, some other physical process must be involved. A tentative explanation has to be found on the fact that close to the edge the low energy electrons are promoted above the Fermi level but cannot easily escape into the vacuum.

4. Tip detection of X-rays absorption

We discuss here the possibility of selecting an individual particle or a specific region of the sample and measure its X-ray absorption with the AFM tip. Figure 3 shows the in-situ AFM topography image of a typical sample consisting of SiGe islands (86% Si, 14% Ge) with $1 \mu m$ width and 500 nm height epitaxially grown on a silicon substrate.

Figure 4a shows the evolution of the tip current as the beam is moved from the tip to the sample. At the beginning, the signal is due to photoemission *from the tip* (region I). Corresponding phase is close to 180° . As the beam is moved toward the sample to a position between the tip and the sample (region II), a minimum is observed. Moving further the beam into the region of the sample below the tip results in a maximum of signal (region III) due to photoemission from the sample *into the tip*. The corresponding phase has shifted 180° indicating a reversal in the direction

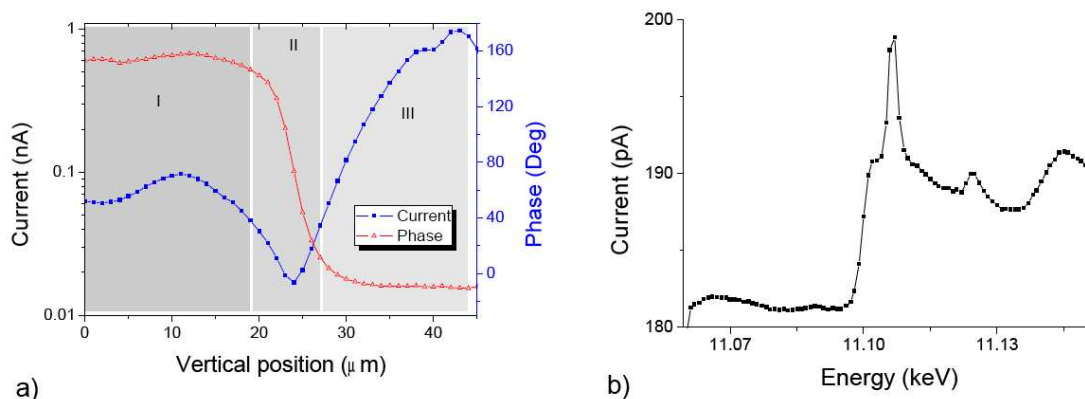


Figure 4. (a) Evolution of the current as the beam is moved from the tip to the sample: (I) beam incident on the tungsten tip, (II) beam passing between the tip and the sample, (III) beam illuminating sample. (b) Ge L_3 edge measured with the tip in total electron yield mode.

of the current. This confirms the assumption that it is possible to distinguish, using the phase of the lock-in, whether photons or photoelectrons are being measured.

The current flowing from the sample into the tip is higher than the current photoemitted from the tip. This is due to the fact that even if the absorption coefficient of the sample is smaller than that of the tungsten tip, the grazing incidence (2°) of the X-ray on the sample produces more shallow electrons which can consequently escape more easily. Analysis of a TEY sample scan for a photon energy above the edge did not permit to evidence any chemical contrast when passing over the SiGe islands. This is only partially due to the low concentration of germanium on the islands. As it will be discussed below, bare tips collect all the electrons emitted within the X-ray beam footprint and engineering efforts have to be put in manufacturing tips for these measurements.

The X-ray absorption signal from the GeSi islands was instead easily detected. For this, the tip was lifted to about $10\ \mu\text{m}$ and the current measured while the beam energy was varied across the germanium K-edge. The result is presented in figure 4b where the current flowing into the tip is plotted as a function of the photon energy.

From the data, it is possible to observe that the SiGe islands were quite oxidized as indicated by the presence of the shoulder before the white line peak [18]. The data was good enough to observe the Extended X-ray Absorption Fine Structure oscillations [19].

The edge jump is of about 10 pA which corresponds to about 5% of the signal. Since ≈ 10 islands were illuminated, each one contributed with about 1 pA. Given the geometry, the solid angle of collection is $\approx \pi/3$ sr mapping then only 1/10 of the total electron yield.

Currently, we are developing "Smart Tips" consisting of tungsten etched tips isolated down to the apex leaving only a very small opening (≈ 50 nm) at the extremity. With these tips put closer to the particles (larger solid angle) the expectation is that islands at least 10 times smaller can be resolved. Moreover, a "Smart Tip" would dramatically reduce the background increasing the edge jump and allowing a more effective amplification of the signal without saturation.

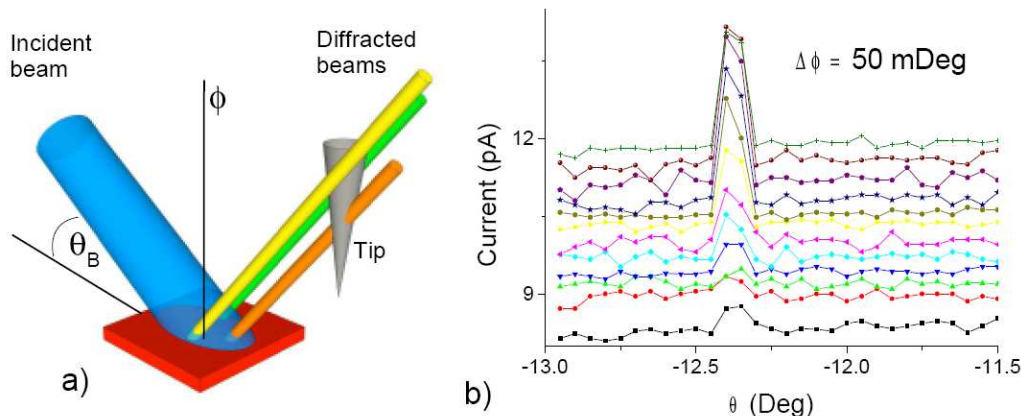


Figure 5. (a) scheme illustrating how different diffracting areas can be resolved. (b) Photocurrent from the tungsten tip as a function of the incidence angle θ and azimuthal ϕ .

5. Tip measurement of the diffraction

We discuss here the possibility of locally measuring Bragg reflections by directly using the tip as a localized photon beam detector. In typical diffraction experiments, the detector is located about one meter away from the sample and collects photons in a very small solid angle in order to provide a very high angular resolution. To study in this way the atomic structure of a single dot requires an X-ray beam with dimensions such that only that dot is illuminated. Otherwise, as many dots are in Bragg condition, the detected signal average over the ensemble of the illuminated dots. The use of a conventional tungsten tip to detect the diffracted beams, cannot give the same angular resolution of a far field detector, but it can give instead a very high *spatial* resolution capable of resolving beams diffracted from different nano-areas even using a wide X-ray beam as sketched in figure 5a. This new technique has been applied to the sample shown in figure 3. The direction normal to the crystal surface is the $\langle 001 \rangle$ and the reflection used is the (002).

The coarse alignment of the SiGe (002) crystal planes for energies of about 11 keV corresponds to an incident angle θ_b of about 12° . The peak hunting for this reflection has been carried out using exclusively the AFM tip scanning θ for a set of different azimuthal angles ϕ (figure 5b).

The Bragg conditions are met at $\theta = 12.35^\circ$ and $\phi = 88.7^\circ$. Figures 6a and 6b show respectively the AFM topography and the tip current image of the sample simultaneously acquired while in Bragg conditions. The small but significant contrast of figure 6b disappears completely when the sample is not in Bragg conditions. The contrast, even if small (0.2%, ≈ 2 pA), evidences a clear correspondence between the topographic image and the current image.

The islands are seen as darker holes, since the photons diffracted from the individual islands and impinging on the tip extract electrons away, which causes a decrease in the overall current which is mainly due to the electrons photoemitted from the sample.

The AFM image is distorted because of a tip effect. The sample being the same as in figure 3, the systematic deformation has to be attributed to the tip which became blunt after several hours of usage in an environment where strong vibrations are present.

The contrast observed as the tip cuts through the array of diffracted beams would be strongly

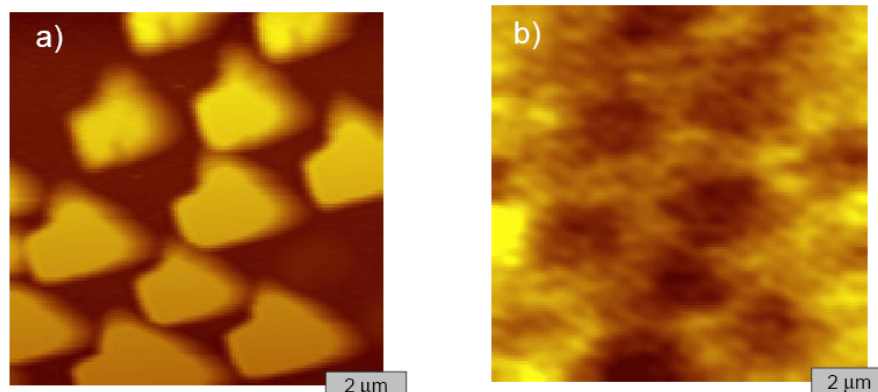


Figure 6. (a) AFM topography image; (b) current image, the darker contrast shows the SiGe islands.

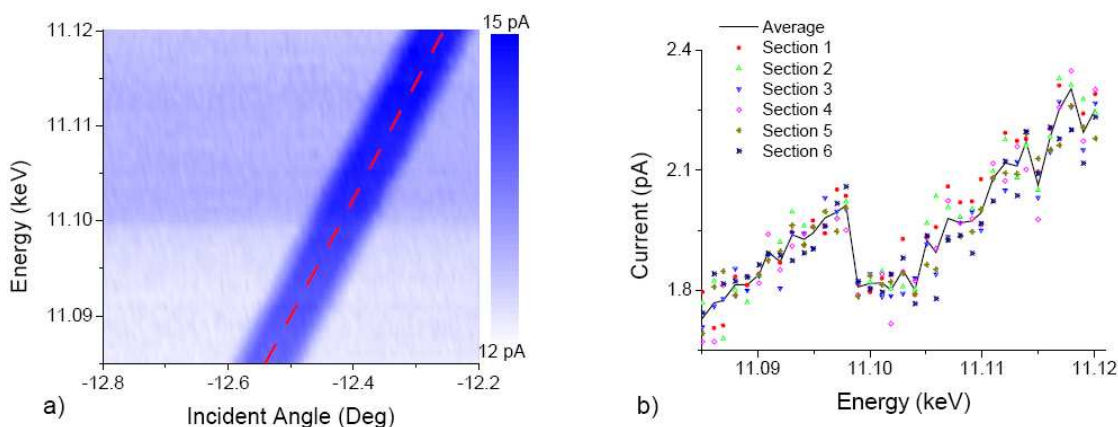


Figure 7. (a) Evolution of the Bragg peak intensity as a function of angle and energy; (b) Cross sections along the stripe on a); the solid line is the average.

enhanced using a "Smart Tip" since it would strongly decrease the background of photoelectrons. It would also prevent photoelectrons generated in the tip, far from its apex (along the z direction), to escape away thus increasing the angular resolution in the scattering plane.

To further emphasize the versatility of this instrument we have used the tip to locally measure the anomalous contribution to the diffraction. Near the absorption edges there is a modification of the scattered intensity due to the absorption processes. The number of photons being diffracted has a sudden decrease due to the sudden increase of the absorption cross section. This gives the opportunity to measure the X-ray Absorption Fine Structure, as seen by a particular Bragg reflection. It is often used to disentangle the Absorption Fine Structure contribution from a given atomic species but distributed in different crystal lattices. This technique is called Diffraction Anomalous Fine Structure [20] and is often used in nanoscience [21]. In figure 7a it is shown the evolution of the Bragg peak as the photon energy is increased.

Figure 7b shows several cross sections (as indicated by the red line on 7a) following the Bragg peak evolution, i.e., the Diffraction Anomalous Fine Structure spectrum. The sections are centered

around the middle of the stripe on figure 7a separated by about 0.01 Deg. This is a preliminary result, but shows that local anomalous diffraction can be measured from a single nanodot with the AFM tip.

In the present experimental conditions, without "Smart Tips" the background due to sample photoemission is the major source of noise. In figure 7b a background of about 12 pA, due to sample photoemission has been subtracted. Note that the subtracted background is not constant throughout the image since it also depends on the photon energy.

6. Perspectives

We are assisting to continuous progresses on "Smart Tips" developments. With this tips, its very likely that it will be possible to obtain spectroscopy and diffraction data with a quality similar to that obtained using more conventional instrumentation but with a lateral resolution about 100 times better.

The tip can be used also for mechanical interaction under X-ray beams. In collaboration with another group, we measured the diffraction from an individual nano-crystal while nano-indenting it with the AFM up to deform it plastically. This will probably be the way to asses a number of mechanical properties of nano-objects and link them to physical and chemical X-ray characterization.

With the current trend toward Synchrotron Radiation "nanobeams" it will be increasingly harder to tell which part of the sample is being investigated. It then seems that the techniques described here will have an important impact also in this context.

Acknowledgments

We thank D. Wermeille from ID3 ESRF for his help at the beam line. We thank T. H. Metzger, C. Mocuta and K. Mundboth from ID1 at ESRF for discussions. This work was supported by the E.U. FP6 program, under contract STRP 505634-1 X-tip and the Portuguese Foundation for Science and Technology for its financial support.

References

- [1] G. Binnig and H. Rohrer, *Scanning tunneling microscopy — from birth to adolescence*, *Rev. Mod. Phys.* **59** (1987) 615.
- [2] J.K. Gimzewski, R. Berndt and R.R. Schlittler, *Observation of local photoemission using a scanning tunneling microscope*, *Ultramicroscopy* **42–44** (1992) 366.
- [3] A. Saito et al., *Development of a scanning tunneling microscope for in situ experiments with a synchrotron radiation hard-X-ray microbeam*, *J. Synchrotron Radiat.* **13** (2006) 216.
- [4] T. Eguchi et al., *Element specific imaging by scanning tunneling microscopy combined with synchrotron radiation light*, *Appl. Phys. Lett.* **89** (2006) 243119.
- [5] T. Matsushima, *Development and trial measurement of synchrotron-radiation-light-illuminated scanning tunneling microscope*, *Rev. Sci. Instrum.* **75** (2004) 2149.
- [6] M. Ishii, *X-ray absorption fine structure measurement using a scanning capacitance microscope: Trial for selective observation of trap centers in the nm region*, *Jpn. J. Appl. Phys.* **41** (2002) 4415.

- [7] C.C. Williams, W.P. Hough and S.A. Rishton, *Scanning Capacitance Microscopy on a 25 nm scale*, *Appl. Phys. Lett.* **55** (1989) 203.
- [8] P. Girard, *Electrostatic force microscopy: principles and some applications to semiconductors*, *Nanotechnology* **12** (2001) 485.
- [9] M. Nonnenmacher, M.P. O'Boyle and H.K. Wicramasinghe, *Kelvin probe force microscopy*, *Appl. Phys. Lett.* **58** (1991) 2921.
- [10] G. Binnig, C.F. Quate and C. Gerber, *Atomic force microscope*, *Phys. Rev. Lett.* **56** (1986) 930.
- [11] F.J. Giessibl, *Advances in atomic force microscopy*, *Rev. Mod. Phys.* **75** (2003) 949.
- [12] D. Rugar et al., *Magnetic Force Microscopy: General principles and application to longitudinal recording media*, *J. Appl. Phys.* **68** (1990) 1169.
- [13] *X-Tip*, European FP6 project, STRP 505634-1 (2004–2007), <http://213.175.108.134/xtip/>.
- [14] E. Betzig, P.L. Finn and J.S. Weiner, *Combined shear force and near-field scanning optical microscopy*, *Appl. Phys. Lett.* **60** (1992) 2484.
- [15] K. Karrai and R.D. Grober, *Piezoelectric tip-sample distance control for near field optical microscopes*, *Appl. Phys. Lett.* **66** (1995) 1842.
- [16] F.J. Giessibl, S. Hembacher, H. Bielefeldt and J. Mannhart, *Subatomic Features on the Silicon (111)-(7 × 7) Surface Observed by Atomic Force Microscopy*, *Science* **289** (2000) 422.
- [17] M. Kulawik et al., *A double lamellae dropoff etching procedure for tungsten tips attached to tuning fork atomic force microscopy/scanning tunneling microscopy sensors*, *Rev. Sci. Instrum.* **74** (2003) 1027.
- [18] R.B. Gregor, F.W. Lytle, J. Kortright and A. Fischer-Colbrie, *Determination of the structure of GeO₂-SiO₂ Glasses by EXAFS and X-ray Scattering*, *J. Non-Cryst. Solids* **89** (1987) 311.
- [19] F.W. Lytle, G.H. Via and J.H. Sinfelt, *Synchrotron Radiation Research*, H. Winick and S. Doniach eds., Plenum, New York (1980) pg. 401.
- [20] H. Stragier, J.O. Cross, J.J. Rehr, L.B. Sorensen, C.E. Bouldin and J.C. Woicik, *Diffraction anomalous fine structure: A new x-ray structural technique*, *Phys. Rev. Lett.* **69** (1992) 3064.
- [21] C. Lamberti, *Characterization of Semiconductor Heterostructures and Nanostructures*, Carlo Lamberti ed., Elsevier (2008) [ISBN: 0444530991].